The published version of the paper "Wang, X., Lin, J., Keramat, A., Ghidaoui, M.S., Meniconi, S., and Brunone, B. (2019). Matched-Field Processing for Leak Detection in a Viscoelasticity Pipe: An Experimental Study. Mechanical Systems and Signal Processing, 124, 459-478." is available at: https://doi.org/10.1016/j.ymssp.2019.02.004

Matched-field processing for leak localization in a viscoelastic pipe: An experimental study

Xun Wang[a], Jingrong Lin[a], Alireza Keramat[a], Mohamed S. Ghidaoui[a], Silvia Meniconi[b], Bruno Brunone[b]

[a] *Department of Civil and Environmental Engineering, Hong Kong University of Science and Technology, Clear Water Bay, Hong Kong, China*
[b] *Department of Civil and Environmental Engineering, University of Perugia, 06125 Perugia, Italy*

Abstract

This paper applies the matched-field processing (MFP) method to leakage localization in a viscoelastic pipe. The viscoelasticity of pipe wall is included in the governing equations of transient wave via the generalized Kelvin-Voigt model and its effect is finally translated into a frequency-dependent wave speed. Then, a leak is localized by MFP via a 1D search of leak location along the pipe, independent of the leak size. Transient experiments with viscoelastic pipe in the Water Engineering Laboratory at University of Perugia and in the Water Resources Research Laboratory at Hong Kong University of Science and Technology are studied. Experimental results demonstrate that the inclusion of pipe wall viscoelasticity and using more frequencies (instead of using only resonant frequencies) improve significantly the leak localization accuracy. It is shown that the MFP leak localization is accurate even for a small leak (the flow ratio of leak and main pipe is approximately 10%) in a noisy environment: among 50 transient experiments, the maximum error of MFP leak localization is only 1.14 m and in the other 49 experiments the error is always lower than 1 m.

Keywords: transient wave, leakage localization, matched-field processing, pipe viscoelasticity, complex environment

1. Introduction

Leakage in water supply systems results in financial losses from wastage of water and health risks since leaks are potential entry points for contaminants during low pressure intrusion events [1]. Since 1980s, fluid transient-based defect detection methodology has been used for leakage detection. It introduces hydraulic pressure waves, measures pressure response at specified location(s), and uses the information of reflection and damping due to leakages to estimate their locations in water pipe systems. Specific methodological examples of this approach are: (i) transient reflection-based method (TRM), such as [2–7]; (ii) transient damping-based method (TDM) by [8]; (iii) frequency response-based method (FRM) by [9–25]; and (iv) inverse transient analysis (ITA) method [26–29].

Real water supply pipeline system is often a highly noisy environment due to traffic, mechanical devices, turbulence, etc. While previous methods in the literature do not theoretically or analytically study the effect of noise using a probabilistic framework, a recent method, known as the matched-field processing (MFP) [21], estimate a leak based on the maximum signal-to-noise ratio (SNR) meaning that the MFP method provides precise localization estimates even in noisy environments. MFP is able to use all available frequencies, not just resonant frequencies, and does not need to identify which frequencies are resonant frequencies, such that the leak estimation is more robust. However, the MFP approach in [21] is based on a transient wave model in elastic pipes; its availability in viscoelastic pipes has not been studied.

Viscoelastic pipes, such as polyvinyl chloride (PVC), polyethylene (PE), and high-density polyethylene (HDPE), are ideally applicable in urban water supply systems due to their excellence resilience, low cost, and convenience in construction and maintenance. The viscoelastic effect of pipe deformation during transient pressure behavior has been investigated [30–37]. It is shown that the viscoelastic behavior changes the nature of transient wave. Leak detection methods that can deal with pipe viscoelasticity have been proposed [36, 38]. However, these methods do not consider the effect of noise in their models and may thus not be applicable in a noisy environment.

In the present paper, the viscoelastic effect of pipe wall is included in the transient model, it is found that it can be equivalently quantified by changing the wave speed in the elastic case to be frequency-dependent. Then, MFP can be applied for leakage detection in a viscoelastic pipe; its efficiency is validated via experiments conducted in the Water Engineering Laboratory at University of Perugia and in the Water Resources Research Laboratory at Hong Kong University of Science and Technology. The accuracy of MFP in pipeline leakage localization and additional gain of using more frequencies, instead of only the resonant frequencies, which have been numerically

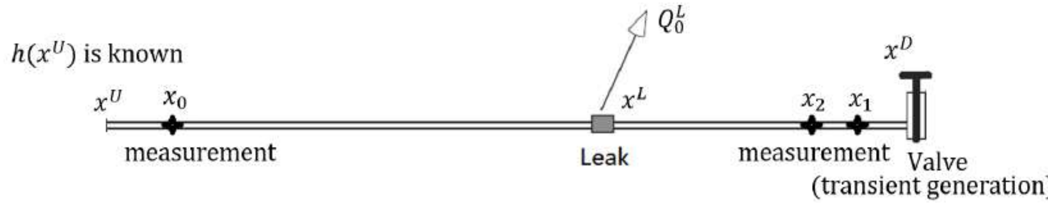

Figure 1: Setup of the pipeline system.

justified via numerical simulation and theoretical analysis in [21, 22], are experimentally illustrated in this paper. Experimental results show that the inclusion of pipe viscoelasticity in the transient model and in the leak detection scheme significantly increases the leak localization accuracy.

The organization of this paper is as follows. It begins with a description of transient wave model in a viscoelastic pipe system in Section 2. Section 3 introduces the MFP method for leak localization. The setups, processing of data, and experimental results are all introduced in Section 4. Based on the experimental results of leak localization, Section 5 discusses the issues of physical model, measurement information, and leak localization algorithm. Finally, conclusions are drawn in Section 6.

2. Transient wave in a viscoelastic pipe

2.1. Governing equations in the time domain

The pipeline configuration is illustrated in Figure 1. The upstream and downstream ends of the single pipe locate at $x = x^U = 0$ and $x = x^D = L$, respectively. The pressure head $h(x^U)$ at x^U is known and a transient generator is placed at x^D. A leak is assumed whose location is denoted by x^L, and z^L, Q_0^L and H_0^L denote the elevation of the pipe at the leak, the steady-state discharge and head at the leak, respectively. The lumped leak parameter $s^L = C^d A^L$ stands for the effective leak size, where C^d is the discharge coefficient of the leak and A^L is the flow area of the leak opening (orifice). The steady-state discharge of the leak is related to the lumped leak parameter by $Q_0^L = s^L\sqrt{2g(H_0^L - z^L)}$, in which g is gravitational acceleration.

For a viscoelastic pipe, the total strain ϵ can be decomposed into an

Nomenclature

q	discharge oscillation
h	pressure head oscillation
x^L	leak location
z^L	pipe elevation at leak
s^L	leak size
Q_0^L, H_0^L	steady-state discharge and head of leak
Q_0	steady-state discharge of main pipe
x_m $(m = 1, \cdots, M)$	sensor coordinate
$\mathbf{\Delta h}$	head difference
$\mathbf{n}$	measurement noise
a_0	wave speed in elastic pipes
a_{ve}	wave speed in viscoelastic pipes
A	area of pipeline
l	pipe length
D	pipe diameter
ω	angular frequency
ω_{th}	fundamental frequency
M	sensor number
K	frequency number
FRF	frequency response function
FRM	frequency response-based method
HDPE	high-density polyethylene
K-V	Kelvin-Voigt
MFP	matched-field processing
MFP-E	MFP based on the model of elastic pipe [21]
MFP-VE	MFP based on the model of viscoelastic pipe
TDM	transient damping-based method
TRM	transient reflection-based method

instantaneous-elastic strain ϵ_e and a retarded strain ϵ_r, i.e.,

$$\epsilon = \epsilon_e + \epsilon_r. \tag{1}$$

Let $\sigma(t)$ stand for dynamic stress at time t ($\sigma(t) = 0$ for $t \leq 0$), ϵ_e and ϵ_r read [39]:

$$\epsilon_e(t) = J_0 \sigma(t), \tag{2}$$

$$\epsilon_r(t) = \int_0^t \sigma(t-s) \frac{dJ}{ds} ds, \tag{3}$$

in which $J_0 = J(0) = 1/E$ is the instantaneous creep-compliance representing the immediate response of the material, E is the Young's modulus of elasticity of pipe wall, and $J(t)$ is the creep function.

The discharge and pressure head oscillations due to a fluid transient are denoted by q and h. The linearized unsteady-oscillatory continuity and momentum equations with time t and spatial coordinate $x \in [x^U, x^L) \cup (x^L, x^D]$ [33, 34] are

$$\frac{\partial q}{\partial x} + \frac{gA}{a_0^2} \frac{\partial h}{\partial t} + 2(1-\nu^2) A \frac{\partial \epsilon_r}{\partial t} = 0 \tag{4}$$

and

$$\frac{1}{gA} \frac{\partial q}{\partial t} + \frac{\partial h}{\partial x} + Rq = 0. \tag{5}$$

Here,

$$a_0 = \left(\rho \left(\frac{1}{\kappa} + (1-\nu^2) \frac{D}{Ee} \right) \right)^{-\frac{1}{2}} \tag{6}$$

is the elastic component of wave speed, κ and ρ are the bulk modulus and density of water, ν is the Poisson's ratio, D is the pipe diameter, and e is the pipe wall thickness. Furthermore, A is the area of pipeline, R is the steady-state resistance term being $R = (f_{DW} Q_0)/(gDA^2)$ for turbulent flows, f_{DW} is the Darcy-Weisbach friction factor, Q_0 is the steady-state discharge in the pipe. The last term of left hand side of Eq. (4) is due to pipe wall viscoelasticity; it equals to 0 in the elastic case since the creep function $J(t)$ is time-independent. Furthermore, ϵ_r here is the retarded circumferential strain and the influence of axial pipe velocity on Eqs. (4) and (5) is neglected.

Inserting Eq. (3) into Eq. (4) gives

$$\frac{\partial q}{\partial x} + \frac{gA}{a_0^2} \frac{\partial h}{\partial t} + 2(1-\nu^2) A \frac{\partial}{\partial t} \int_0^t \sigma(t-s) \frac{dJ}{ds} ds = 0. \tag{7}$$

Considering the force balance for the stress in the pipe wall and the pressure in fluid, i.e.,

$$2\sigma e = pD, \tag{8}$$

where $p = \rho g h$ is the dynamic pressure, we have

$$\sigma(t) = \frac{\rho g D}{2e} h(t). \tag{9}$$

Therefore, Eq. (7) becomes

$$\frac{\partial q}{\partial x} + \frac{gA}{a_0^2}\frac{\partial h}{\partial t} + (1-\nu^2)\frac{\rho g D A}{e}\frac{\partial}{\partial t}\int_0^t h(t-s)\frac{dJ}{ds}ds = 0. \tag{10}$$

2.2. Governing equations in the frequency domain and wave speed calibration for pipe wall viscoelasticity

Taking a Fourier transform of Eq. (10), it becomes

$$\frac{\partial q}{\partial x} + \frac{gA}{a_0^2}\mathrm{i}\omega h + (1-\nu^2)\frac{\rho g D A}{e}\mathcal{F}\left(\frac{\partial}{\partial t}\int_0^t h(t-s)\frac{dJ}{ds}ds\right) = 0, \tag{11}$$

where $\mathcal{F}(\cdot)$ stands for the operation of Fourier transform. The last term of Eq. (11) can be simplified by the Leibniz's rule for differentiation under the integral sign, the properties of Fourier transform and convolution, and $h(t) = 0$ for $t \leq 0$, as:

$$\begin{aligned}
& \mathcal{F}\left(\frac{\partial}{\partial t}\int_0^t h(t-s)\frac{dJ}{ds}ds\right) \\
= \; & \mathcal{F}\left(h(0)\frac{dJ}{dt} + \int_0^t \frac{\partial h}{\partial t}(t-s)\frac{dJ}{ds}ds\right) = \mathcal{F}\left(\int_0^t \frac{\partial h}{\partial t}(t-s)\frac{dJ}{ds}ds\right) \\
= \; & \mathcal{F}\left(\frac{\partial h}{\partial t}\right)\mathcal{F}\left(\frac{dJ}{dt}\right) = \mathrm{i}\omega h \mathcal{F}\left(\frac{dJ}{dt}\right).
\end{aligned} \tag{12}$$

Here, the creep function $J(t)$ is assumed to follow the generalized Kelvin-Voigt (K-V) model [31]:

$$J(t) = J_0 + \sum_{j=1}^{N_{kv}} J_j(1 - \exp(-t/\tau_j)), \tag{13}$$

where N_{kv} is the truncated order, J_j and τ_j are coefficients of the K-V model. Therefore, we have

$$\frac{dJ}{dt} = \sum_{j=1}^{N_{kv}} \frac{J_j}{\tau_j} \exp(-t/\tau_j) \tag{14}$$

and

$$\mathcal{F}\left(\frac{dJ}{dt}\right) = \sum_{j=1}^{N_{kv}} \frac{J_j}{1 + \mathrm{i}\omega\tau_j}. \tag{15}$$

By Eqs. (12) and (15), Eq. (11) becomes

$$\frac{\partial q}{\partial x} + \frac{gA}{a_{ve}^2}\mathrm{i}\omega h = 0, \tag{16}$$

where

$$a_{ve} = \left(\rho\left(\frac{1}{\kappa} + (1-\nu^2)\frac{D}{e}\left(J_0 + \sum_{j=1}^{N_{kv}} \frac{J_j}{1 + \mathrm{i}\omega\tau_j}\right)\right)\right)^{-\frac{1}{2}}. \tag{17}$$

Furthermore, taking Fourier transform of Eq. (5), we obtain

$$\frac{\partial h}{\partial x} + \left(\frac{\mathrm{i}\omega}{gA} + R\right) q = 0. \tag{18}$$

Eqs. (16) and (18) are respectively the continuity and momentum equations in the frequency domain. In the considered viscoelastic case where the pipe motion is assumed to be purely radial, the momentum equation Eq. (18) is same as the elastic case; the continuity equation changes but it is equivalent to replace the constant wave speed in the elastic case (a_0 in Eq. (6)) by the frequency-dependent a_{ve} in Eq. (17).

2.3. Boundary conditions and data model

Solving Eqs. (16) and (18) with boundary conditions of the discharge $q(x^U)$ and head $h(x^U)$ at x^U, for the case of $x_m < x^L$, the discharge and head (frequency response [40]) at a measurement station x_m can be computed as [41, 42]:

$$\begin{pmatrix} q(x_m) \\ h(x_m) \end{pmatrix} = M^{NL}(x_m) \begin{pmatrix} q(x^U) \\ h(x^U) \end{pmatrix}, \tag{19}$$

in which

$$M^{NL}(x) = \begin{pmatrix} \cosh(\mu x) & -\frac{1}{Z}\sinh(\mu x) \\ -Z\sinh(\mu x) & \cosh(\mu x) \end{pmatrix} \tag{20}$$

is the field matrix,

$$Z(\omega) = \mu a_{ve}^2(\omega)/(\mathrm{i}\omega g A) \tag{21}$$

is the characteristic impedance,

$$\mu(\omega) = a_{ve}^{-1}(\omega)\sqrt{-\omega^2 + \mathrm{i}gA\omega R} \tag{22}$$

is the propagation function. In the case of $x_m > x^L$, by the head and mass conservation condition across the leak:

$$h(x^{L-}) = h(x^{L+}) = h(x^L); \tag{23}$$

$$q(x^{L-}) = q(x^{L+}) + q(x^L) = q(x^{L+}) + \frac{Q_0^L}{2(H_0^L - z^L)}h(x^L), \tag{24}$$

in which x^{L-} and x^{L+} represent respectively just upstream and downstream of x^L, the discharge and head at a measurement station x_m has the form [41, 42]:

$$\begin{pmatrix} q(x_m) \\ h(x_m) \end{pmatrix} = M^{NL}(x_m - x^L)\begin{pmatrix} 1 & -\frac{Q_0^L}{2(H_0^L - z^L)} \\ 0 & 1 \end{pmatrix} M^{NL}(x^L)\begin{pmatrix} q(x^U) \\ h(x^U) \end{pmatrix}. \tag{25}$$

The transfer matrix on the right hand side of Eq. (25) can be further simplified as a form of variable separation of x^L and s^L [21, 22]; the head at $x = x_m$ for a given angular frequency ω_k is [21]:

$$h(\omega_k, x_m) = h^{NL}(\omega_k, x_m) + s^L G(\omega_k, x^L, x_m), \tag{26}$$

wherein

$$h^{NL}(\omega_k, x_m) = -Z_k \sinh(\mu_k x_m)\, q(x^U, \omega_k) + \cosh(\mu_k x_m)\, h(x^U, \omega_k) \tag{27}$$

and

$$\begin{aligned} &G(\omega_k, x^L, x_m) \\ =& \begin{cases} -\frac{\sqrt{g}Z_k \sinh\left(\mu_k(x_m - x^L)\right)}{\sqrt{2(H_0^L - z^L)}}\left(Z_k \sinh\left(\mu_k x^L\right) q(x^U, \omega_k) - \cosh\left(\mu_k x^L\right) h(x^U, \omega_k)\right), & x_m > x^L \\ 0, & x_m \le x^L \end{cases} \end{aligned} \tag{28}$$

Assume that the measured heads at the frequency ω_k ($k = 1 \cdots, K$) and at the location x_m ($m = 1 \cdots, M$) are available and they are assumed to be contaminated by a noise n_{mk}, i.e.,

$$h(\omega_k, x_m) = h^{NL}(\omega_k, x_m) + s^L G(\omega_k, x^L, x_m) + n_{mk}. \tag{29}$$

By denoting

$$\Delta\mathbf{h} = (\Delta h_{11}, \cdots, \Delta h_{1K}, \cdots, \Delta h_{M1}, \cdots, \Delta h_{MK})^\top, \tag{30}$$

where

$$\Delta h_{mk} = h(\omega_k, x_m) - h^{NL}(\omega_k, x_m), \tag{31}$$

$$\mathbf{G}(x^L) = (G(\omega_1, x^L, x_1), \cdots, G(\omega_K, x^L, x_1), \cdots, G(\omega_1, x^L, x_M), \cdots, G(\omega_K, x^L, x_M))^\top, \tag{32}$$

and

$$\mathbf{n} = (n_{11}, \cdots, n_{1K}, \cdots, n_{M1}, \cdots, n_{MK})^\top, \tag{33}$$

we finally have

$$\Delta\mathbf{h} = s^L \mathbf{G}(x^L) + \mathbf{n}. \tag{34}$$

In this paper, $\Delta\mathbf{h}$ is the data for leakage localization algorithm.

Note that in Eq. (28), the boundary conditions at the upstream node $q(x^U)$ and $h(x^U)$ are assumed to be known. Here, $h(x^U)$ at the upstream boundary x^U is known, for example $h(x^U)$ can be reasonably assumed to be $h(x^U) = 0$ if the upstream is connected to a reservoir. The discharge $q(x^U)$ can be estimated if a transducer near the upstream boundary, whose location is denoted by x_0, is available [43, 44]. Assuming there is no leak between x^U and x_0 and using the pressure head measurement $h(x_0)$ at x_0, the discharge $q(x^U)$ at the frequency ω_k can be estimated [22] by

$$\hat{q}(x^U, \omega_k) = \frac{\cosh(\mu_k(x_0 - x^U))h(x^U, \omega_k) - h(x_0, \omega_k)}{Z_k \sinh(\mu_k(x_0 - x^U))}. \tag{35}$$

3. Leak localization using the matched-field processing method

In this section, the leakage localization problem is solved using the MFP method. The noise vector $\mathbf{n}$ is assumed to follow a zero-mean Gaussian distribution $\mathcal{N}(\mathbf{0}, \sigma^2 \mathbf{I}_{MK})$, where $\mathbf{I}_{MK}$ is a MK-dimensional identity matrix. The leakage location can be estimated using MFP via [21]:

$$\widehat{x^L} = \arg \max_{x^L \in (0,l)} \frac{\Delta\mathbf{h}^H \mathbf{G}(x^L)\mathbf{G}^H(x^L)\Delta\mathbf{h}}{\mathbf{G}^H(x^L)\mathbf{G}(x^L)}. \tag{36}$$

Remark that the random noise is assumed to be Gaussian distributed. Since frequency-domain pressure is obtained from discrete Fourier transform, which is a linear combination of measured time-domain pressure signals, thus the frequency-domain noise can be approximately as Gaussian distributed according to the Law of Large Number. A recent experimental investigation [45] also shows that, in a pipe with flow, the Gaussian assumption of noise distribution is reasonable. Furthermore, uncorrelated white noise (the covariance matrix is $\sigma^2\mathbf{I}_{MK}$) is assumed here; if the noise is non-white, a data transformation technique for noise whitening [21] can be applied before implementing MFP such that the white noise assumption still holds and the leakage localization in Eq. (36) can still be used without changing its structure. This noise-whitening technique can improve the leak localization result when noise level is high according to the numerical results in [21].

Note that Eq. (36) implies that a leak can be localized by a 1D search of leak location along the pipe, independent of its leak size. Physically, this is possible because the leak location determines the shape of FRF while the leak size only proportionally changes the magnitude of FRF at different frequencies [15, 46]. Essentially, MFP uses only the shape of FRF [21] such that the influence of leak size can be excluded.

Finally, the MFP algorithm of leakage localization in a viscoelastic pipe is summarized in Algorithm 1.

4. Experimental results

4.1. Experiments at University of Perugia

In this section, the MFP method for leak localization is tested using the water hammer experimental data obtained from the Water Engineering Laboratory of University of Perugia.

4.1.1. Experimental setup

The experimental setup is shown in Figure 2. A HDPE pipe with length $l = 166.28$ m and diameter $D = 0.0933$ m is used. Transient wave is generated by a rapid and full closure of the downstream valve; the time duration of valve closure is approximately 0.1 s. Pressures are measured by three transducers located at $x_0 = 27.7$ m, $x_1 = 68.27$ m, and $x_2 = 166.28$ m, respectively. The average steady-state pressure head (pre-transient) at the upstream reservoir and at the valve are respectively 18.28 m and 17.09 m. The leak location is $x^L = 60.84$ m and the effective leak size is $C^d A^L = 6.8 \times 10^{-5}$ m^2. By

Algorithm 1 Localization of leakage in a viscoelastic pipe using MFP

1. Select K frequencies $\omega_1, \cdots, \omega_K$. The maximum frequency ω_K should not be higher than the maximum probing frequency. It is also suggested to use all available frequencies that are lower than the maximum probing frequency. The maximum probing (angular) frequency can be approximately computed from $2\pi/T_c$ (T_c is the time duration of valve closure) or observed from the spectrum of measured signal.
2. Compute a_{ve} from Eq. (17) for each selected frequency ω_k ($k = 1, \cdots, K$), in which the viscoelastic coefficients N_{kv}, J_j and τ_j ($j = 1, \cdots, N_{kv}$) of the generalized K-V model are used and obtained prior to the transient test with leak.
3. Estimate the boundary condition $\hat{q}(x^U, \omega_k)$ for each selected frequency ω_k from Eq. (35) using the pressure head measurements from x_0.
4. Calculate $h^{NL}(\omega_k, x_m)$ via Eq. (27) and use the head differences $\Delta\mathbf{h}$ as the data, which includes pressure heads from K frequencies and M sensors $(x_1, \cdots, x_M)$.
5. Plot the objective function in Eq. (36):

$$|B|^2 = \frac{\Delta\mathbf{h}^H \mathbf{G}(x^L)\mathbf{G}^H(x^L)\Delta\mathbf{h}}{\mathbf{G}^H(x^L)\mathbf{G}(x^L)}. \tag{37}$$

with respect to x^L and retain x^L corresponding to maximum $|B|^2$ as leak location estimate.

(a)

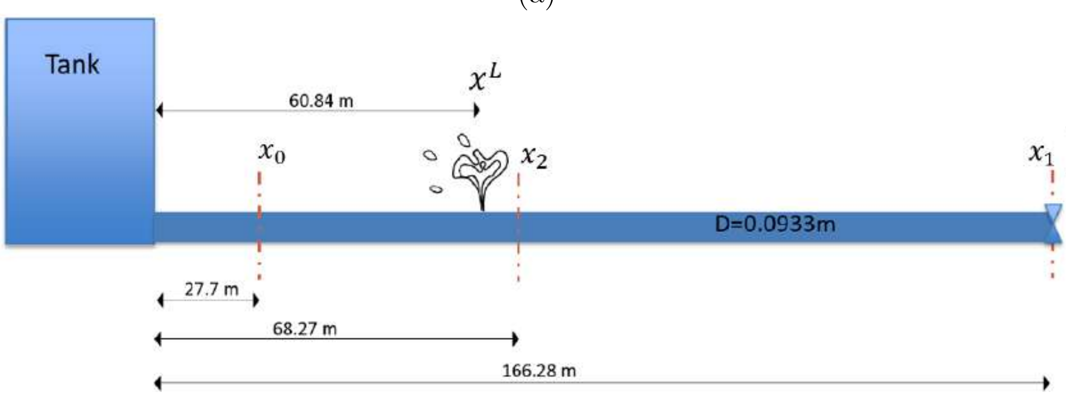

(b)

Figure 2: (a) Photo and (b) sketch map of pipe transient experiment in the Water Engineering Laboratory at University of Perugia.

computing the travel time of the wave between the transducers, the wave speed is estimated as $a_0 = 375$ m/s. The Darcy-Weisbach friction factor is also computed from the measured head loss as $f_{DW} = 0.0233$.

4.1.2. Post-processing of measurements

The measured heads in time from the three sensors are shown in Figure 3. Their system frequency response functions (FRFs) are obtained as follows.

- Computing the FRF requires both the output from the system (the measured pressure head of transient wave in Figure 3) and the input signal sent to the system. The latter is computed by selecting only the first step rise (from the last steady-state point to the maximum of the first jump) of the measurement and keeping it constant after the maximum point [47], since the input signal is generated by the full closure of valve. Figure 4 (a) takes the measurement from x_1 as an example which displays the measured head and the computed input signal.

- Note that these step time-series signals have infinite energy in theory (their integral from $-\infty$ to $+\infty$ equals to infinity), such that their spectra cannot be produced by a conventional Fourier transform [48]. Therefore, in order to change the signals into a finite energy form, each step signal is modified to a pulse-type signal by computing the difference between the original signal and its delay. The delay of the measurement or the input signal is computed by delaying the original signal with a time lag being longer than the time from the last steady-state point to the maximum of the first jump and being shorter than the time for the first reflection to arrive at the measure station [47]. The accuracy of this correction procedure does not depend on the time lag factor if it is in this range. Figure 4 (b) and (c) show the original signals and their delays of the measurement and the input, while Figure 4 (d) displays the differences (impulse-type signals) of the measured head and the input signal. According to the additive and distributive nature of time invariant linear systems, the frequency response of the system remains unchanged as a result of this operation (cf. Eq. (5.21) in [47]).

- Then, conventional Fourier transform is applied to the impulse-type output and input signals, which gives the corresponding frequency do-

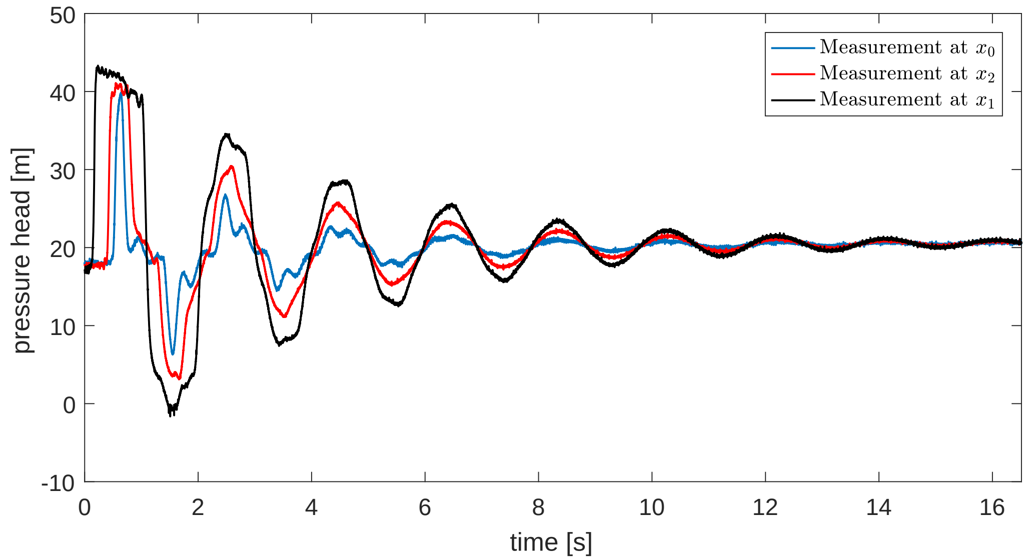

Figure 3: Measured pressure in the time domain from the three transducers.

main signals. Finally, the system FRF is obtained by their quotient. The FRFs obtained from the three sensors are shown in Figure 5.

4.1.3. Leak localization results

$\nu = 0.43$	$\kappa = 2.1 \times 10^9$ Pa	$\rho = 10^3$ kg/m^3
$D = 93.3 \times 10^{-3}$ m	$e = 7.5 \times 10^{-3}$ m	$J_0 = 0.68 \times 10^{-9}$ Pa^{-1}
$J_1 = 0.951 \times 10^{-10}$ Pa^{-1}	$\tau_1 = 0.05$ s	$J_2 = 1.065 \times 10^{-10}$ Pa^{-1}
$\tau_2 = 0.5$ s	$J_3 = 0.815 \times 10^{-10}$ Pa^{-1}	$\tau_3 = 1.5$ s

Table 1: Coefficients for pipe wall viscoelasticity in the experiments at University of Perugia.

As already stated, the wave speed is estimated by travel time between two transducers and this leads to $a_0 = 375$ m/s. The calibrated frequency-dependent wave speed a_{ve} is obtained from Eq. (17), where the truncated order $N_{kv} = 3$ and the corresponding coefficients J_j and τ_j, $j = 1, 2, 3$, are obtained (shown in Table 1) via a calibration of viscoelastic parameters of

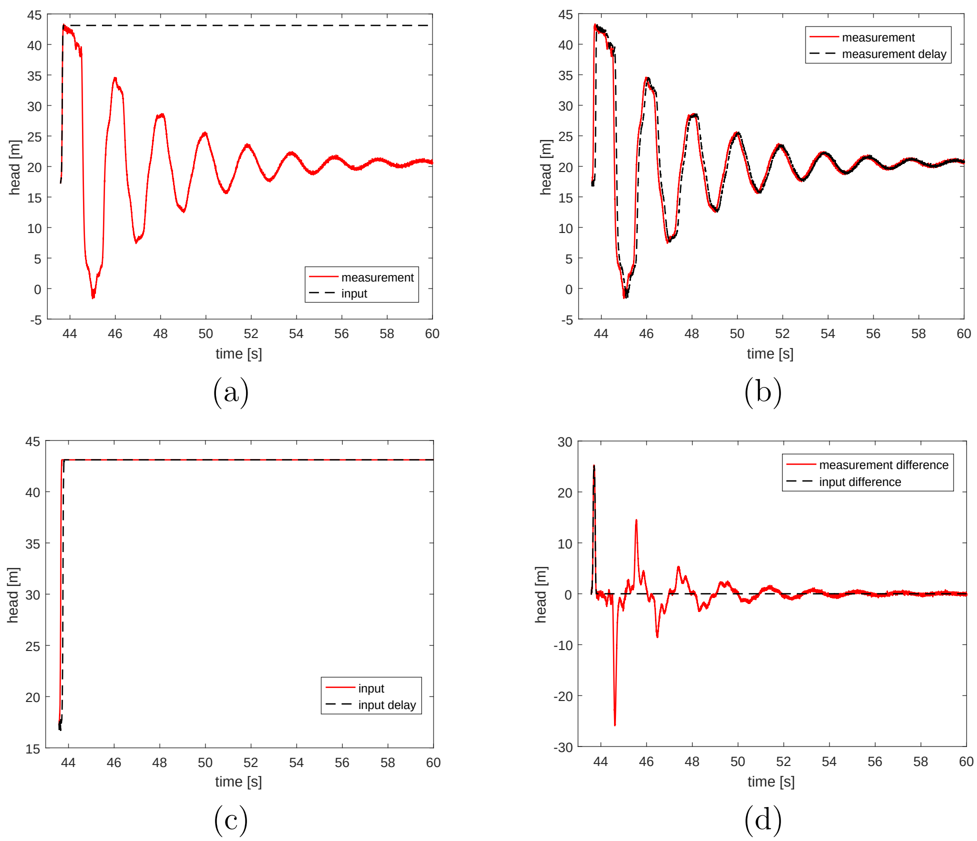

Figure 4: Post-processing of measurement from the transducer at x_1: (a) the measurement and the computed input signal; (b) the measurement and its time delay; (c) the input signal and its time delay; (d) difference of the measurement and its delay and the difference of the input signal and its delay.

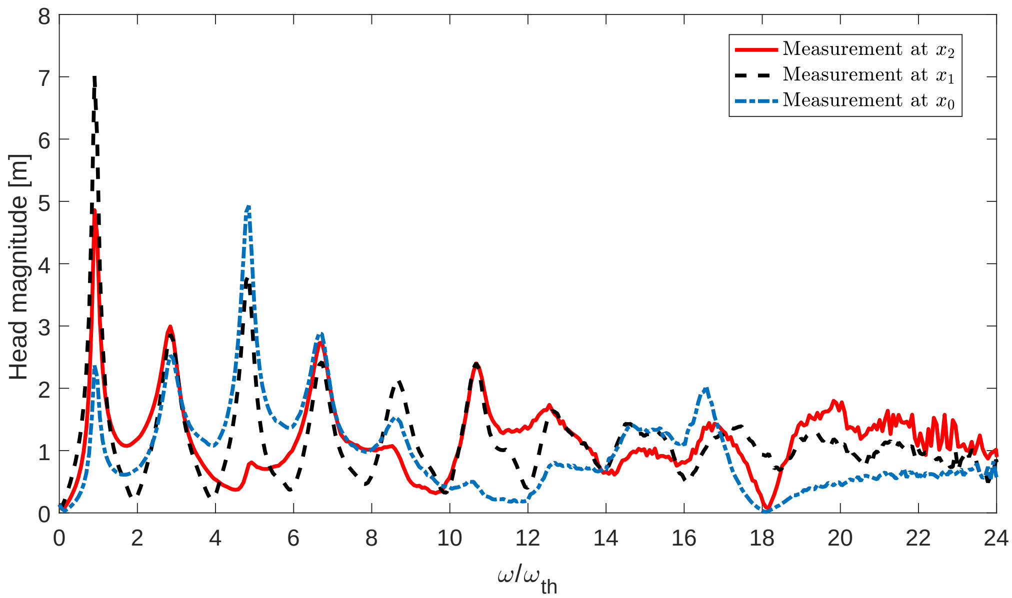

Figure 5: Frequency response function of measurements from the three transducer.

pipe material [49]. More specifically, a transient test without leak is done prior to the leaking test and the viscoelastic parameters are calibrated such that the transient wave model (without leak but J_j and τ_j are free parameters) is closest to the measured data.

In the following, the leak is localized using MFP. The leak detection results with and without the viscoelastic terms are both shown. To avoid confusion, we denote MFP-E as the MFP method based on the model of elastic pipe that does not include the viscoelastic terms (i.e., the method in [21]) and MFP-VE as the viscoelastic version of MFP proposed in the present paper. In MFP-E, the wave speed is $a_0 = 375$ m/s.

The upstream discharge $q(x^U)$, which appears in both h^{NL} and G in Eq. (34), is estimated via Eq. (35), in which $h(x_0)$ is the frequency response from the upstream transducer $x_0 = 27.7$ m. The choice of frequencies is an important issue for MFP. First, the maximum frequency included in the data $\Delta\mathbf{h}$ (or bandwidth) should be decided. In Figure 5, the shape of FRF can be clearly seen for low frequencies, but the signal of transient wave becomes weak as the frequency increases. As a matter of fact, it can be observed from Figure 5 that the data of FRF are not reliable when $\omega/\omega_{th} > 15$ in this experiment and is mainly comprised of noise. Second, the number of used frequency (in the given frequency range) also affects the localization results. It has been shown in [21] that with a given bandwidth using more frequencies increases the robustness of leak localization, particularly in a noisy environment.

Figure 6 shows the leak localization results using MFP. Here, the used angular frequencies are denoted by $\{\omega : \omega_{th}, \omega_{th} + \Delta\omega, \omega_{th} + 2\Delta\omega, \cdots, n\omega_{th}\}$. Figure 6 (a) and (b) displays the results for $n = 13$ (i.e., seven peaks in FRFs) and $\Delta\omega = \omega_{th}/7$ (i.e., in total 85 frequencies are used) using MFP-E and MFP-VE, respectively. It is clear that the model without viscoelasticity leads to a bias of leak localization (the error is 1.74 m) and the the model with viscoelasticity improves the precision (the error is 0.66 m). This illustrates the importance of including viscoelasticity in the detection scheme. Figure 6 (c) and (d) shows the corresponding results with resonant frequencies only. In the case without including pipe viscoelasticity, a higher peak of MFP objective function appears near the downstream end of the pipe which results in a wrong estimate of leak location. The result is better when the viscoelasticity is considered but the error (1.76 m) is still larger than using more frequencies (0.66 m in Figure 6 (b)).

The localization error with different frequency bandwidth ($n = 5, 7, \cdots, 17$)

and frequency step size ($\Delta\omega = \omega_{th}/7, \omega_{th}/2, \omega_{th}, 2\omega_{th}$) are shown in Figure 7. These results clearly show that MFP-VE improves the leak localization accuracy. Furthermore, this figure justifies that using more frequencies in a given range decreases the localization error. In the cases where $\Delta\omega = \omega_{th}/7, \omega_{th}/2$, the error is always less than 5 m (labeled by the dotted lines in Figure 7) for all the frequency ranges except $n = 5$ where too little information is available. By contrast, only using resonant (or even with anti-resonant frequencies together) obviously increases the error; including viscoelasticity becomes more important and the choice of frequency range must be careful. The working frequency (here, "working" means the localization error is less than 5 m) for the four cases of frequency densities is listed in the second column of Table 2. This table also displays the average error for each $\Delta\omega$ in the corresponding working range of frequency, which illustrates again the importance of including viscoelasticity in the leak detection scheme and using more frequencies.

$\Delta\omega$	n	average error [m]	
		MFP-E	MFP-VE
$2\omega_{th}$	$7-11$	1.39	0.89
ω_{th}	$7-13$	1.21	0.99
$\omega_{th}/2$	$7-17$	1.04	0.72
$\omega_{th}/7$	$7-17$	0.96	0.58

Table 2: The chosen maximum frequency such that the leak localization error less than 5 m (represented by n in the second column) and the average error of leak localization in the corresponding frequency range with various frequency spacing $\Delta\omega = 2\omega_{th}, \omega_{th}, \omega_{th}/2, \omega_{th}/7$.

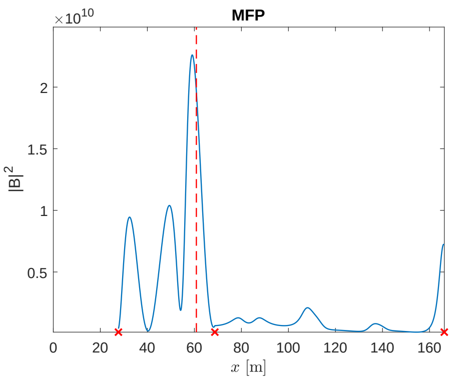

(a) $\Delta\omega = \omega_{th}/7$, MFP-E

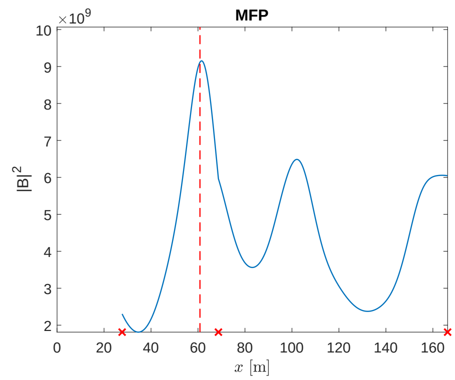

(b) $\Delta\omega = \omega_{th}/7$, MFP-VE

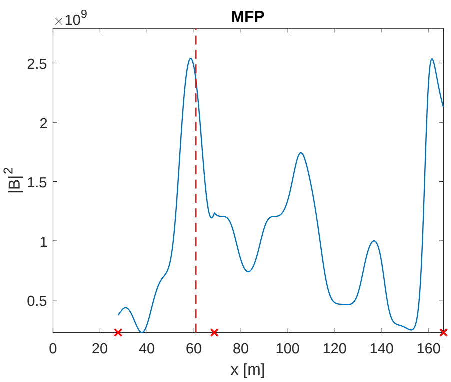

(c) $\Delta\omega = 2\omega_{th}$, MFP-E

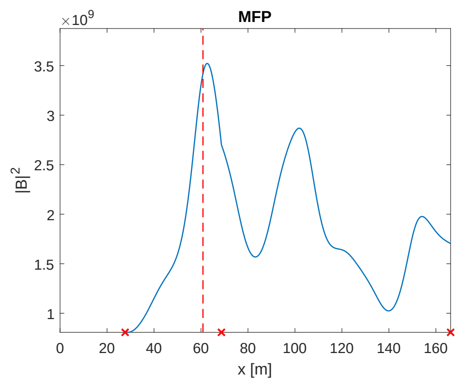

(d) $\Delta\omega = 2\omega_{th}$ MFP-VE

Figure 6: Leak localization using MFP with different frequency spacing: (a,b) $\Delta\omega = \omega_{th}/7$ (i.e., in total 85 frequencies are used) and (c,d) $\Delta\omega = 2\omega_{th}$ (resonant frequencies only; in total 7 frequencies). In subfigures (a,c) and subfigures (b,d), the results are obtained with MFP-E and MFP-VE, respectively. The crosses and dash lines represent the sensor and actual leak locations, respectively.

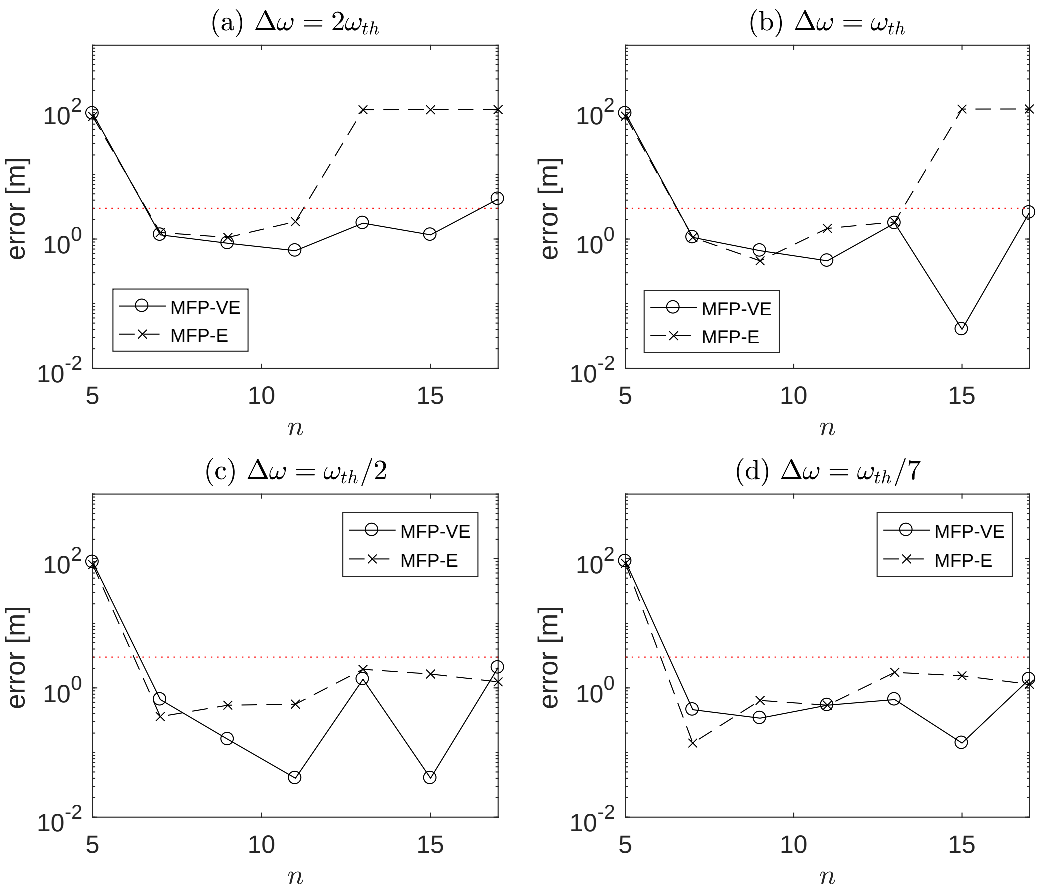

Figure 7: Leak localization error with different frequency spacing (a) $\Delta\omega = 2\omega_{th}$ (resonant frequencies only); (b) $\Delta\omega = \omega_{th}$ (resonant and anti-resonant frequencies); (c) $\Delta\omega = \omega_{th}/2$; and (d) $\Delta\omega = \omega_{th}/7$. The solid and dash lines respectively stand for MFP-E and MFP-VE.

4.2. Experiments at Hong Kong University of Science and Technology

This section applies the MFP leak localization method to the experimental results obtained from the newly-built water pipe system at the Water Resources Research Laboratory at Hong Kong University of Science and Technology.

4.2.1. Experimental setup and measurements

The setup of HDPE pipeline system is shown in Figure 8. The pipe length is $l = 144$ m and its diameter is $D = 0.0792$ m. A pump (in Figure 8 (a) middle), instead of the surge tank used in the experiments conducted at University of Perugia, is connected to the upstream of pipe. A downstream valve is used to generate transient waves; the time closure is approximately 0.05 s. Three hydrophones at $x_0 = 36.92$ m, $x_1 = 141.43$ m and $x_2 = 122.25$ m are set in the pipe to measure pressure. A leak locates at $x^L = 45.58$ m (in Figure 8 (a) right); the leak size can be changed via different valve settings. Three different leak sizes are tested, as shown in Figure 9, because leak size is crucial in terms of leak detectability [50]. The three tests correspond to the following steady-state flow ratio of leak and main pipe: $Q_0^L/Q_0 = 40\%, 20\%, 10\%$. The leak flow Q_0^L and the pipe flow Q_0 are measured from two flow meters just upstream and just downstream of the leak.

Figure 10 (a) shows three different measured pressure head signals (i.e., from three different water hammer experiments) at $x_1 = 141.43$ m, where $Q_0^L/Q_0 = 40\%$. It can be seen from this figure that the measured signal is much more noisy and aleatory, and has more uncertainties than those in Figure 3 (experiments at University of Perugia). A similar phenomenon can be observed by the corresponding FRF in Figure 10 (b), which is also much more noisy than those in Figure 5. This may be partially due to the pump, which itself generates much noise. The presence of the noise and uncertainty makes the leak localization more challenging:

- In Measurement 2 in Figure 10 (a), the pressure drop due to leak is not obvious even if the leak is large ($Q_0^L/Q_0 = 40\%$). This unclear reflection due to leak may mean that some reflection-based leak detection methods fail.

- In Measurement 3 in Figure 10 (a), a very strong noise can be seen in the first period of time signal, which may disturb some signal processing techniques.

(a)

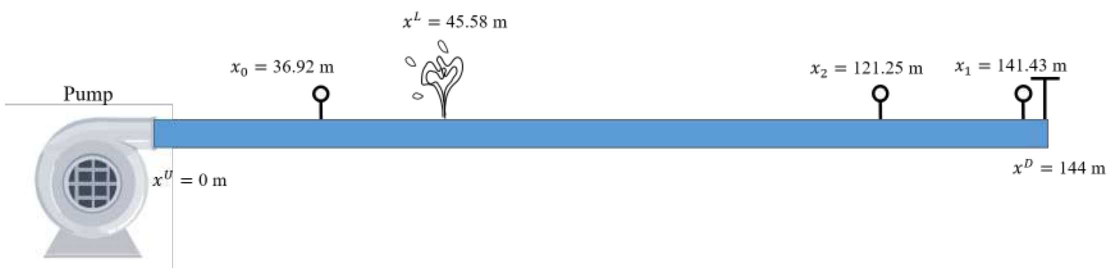

(b)

Figure 8: (a) Photos (pipe (left), pump (middle), and leak (right)) and (b) sketch map of pipe transient experiment in the Water Resources Research Laboratory at Hong Kong University of Science and Technology.

Figure 9: Photos of three different leak sizes in the HKUST experiments. The flow rate ratio between the main and the leak is approximately 40% (left), 20% (middle), and 10% (right)

- The FRFs in Figure 10 (b) are noisy and the resonant frequencies are not so clear as in the experiments at University of Perugia (cf. Figure 5). This poses a challenge for methods based on resonant frequencies.

Moreover, the MFP method needs $\hat{q}(x^U)$ which is estimated via Eq. (35). Here, it is assumed $h(x^U) = 0$ in the computation of Eq. (35). However, unlike the experiments in Section 4.1 where a reservoir is connected to the pipe upstream to keep the pressure head constant, in the experiments in this section a pump is used such that the assumption $h(x^U) = 0$ could result in uncertainties in the model.

4.2.2. Leak localization results

Figure 11 shows the MFP leak localization results using the signals in Figure 10. Here, the frequencies used are all available frequencies from ω_{th} to $17\omega_{th}$. The MFP without viscoelastic calibration (MFP-E) results in bad results; in Figure 11 (a,c,e), many peaks with almost equal height appear in the MFP objective function. However, the leak can be accurately localized by the proposed MFP with consideration of viscoelasticity (MFP-VE), where the coefficients of viscoelasticity are displayed in Table 3, for all the three measurements (the error is 0.14 m, 0.96 m and 0.26 m, respectively), which illustrate the robustness of the proposed method with respect to noise and uncertainties.

$\nu = 0.43$	$\kappa = 2.1 \times 10^9$ Pa	$\rho = 10^3$ kg/m^3
$D = 79.2 \times 10^{-3}$ m	$e = 5.4 \times 10^{-3}$ m	$J_0 = 4.8 \times 10^{-10}$ Pa^{-1}
$J_1 = 1.957 \times 10^{-10}$ Pa^{-1}	$\tau_1 = 0.038$ s	$J_2 = 1.0954 \times 10^{-10}$ Pa^{-1}
$\tau_2 = 0.6$ s	$J_3 = 9.05 \times 10^{-12}$ Pa^{-1}	$\tau_3 = 1.5$ s

Table 3: Coefficients for pipe wall viscoelasticity in the experiments at Hong Kong University of Science and Technology.

Due to the high level of noise and uncertainty, for each leak size ($Q_0^L/Q_0 = 40\%, 20\%, 10\%$) the experiment is repeated 50 times and the leak localization results are statistically analyzed. Here, we compare MFP-VE and MFP-E with only resonant frequencies and with more frequencies, as well as three representative methods in the literature:

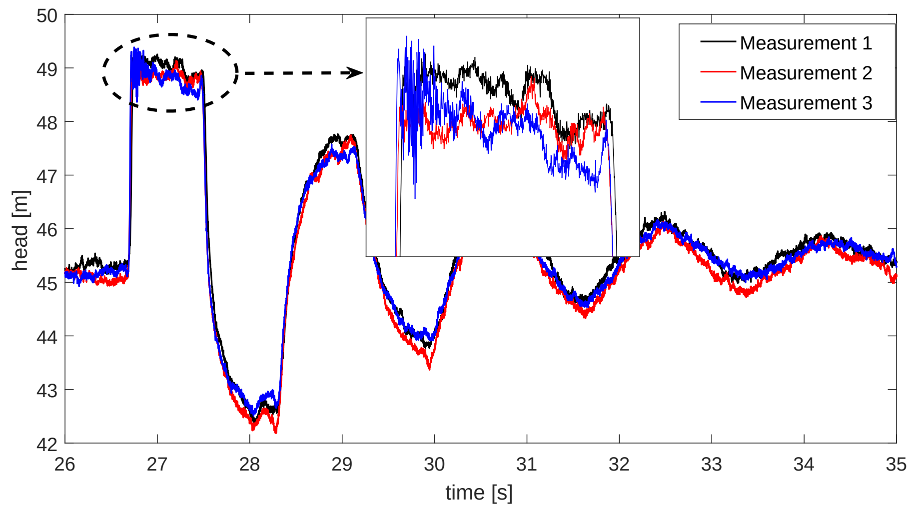

(a)

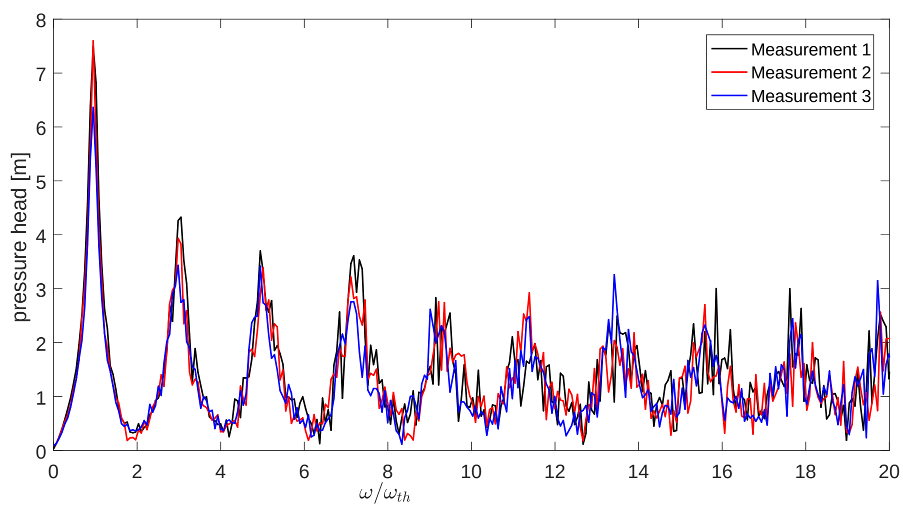

(b)

Figure 10: Three different measurements obtained from the sensor $x_1 = 141.43$ m in the time domain (a) and in the frequency domain (b).

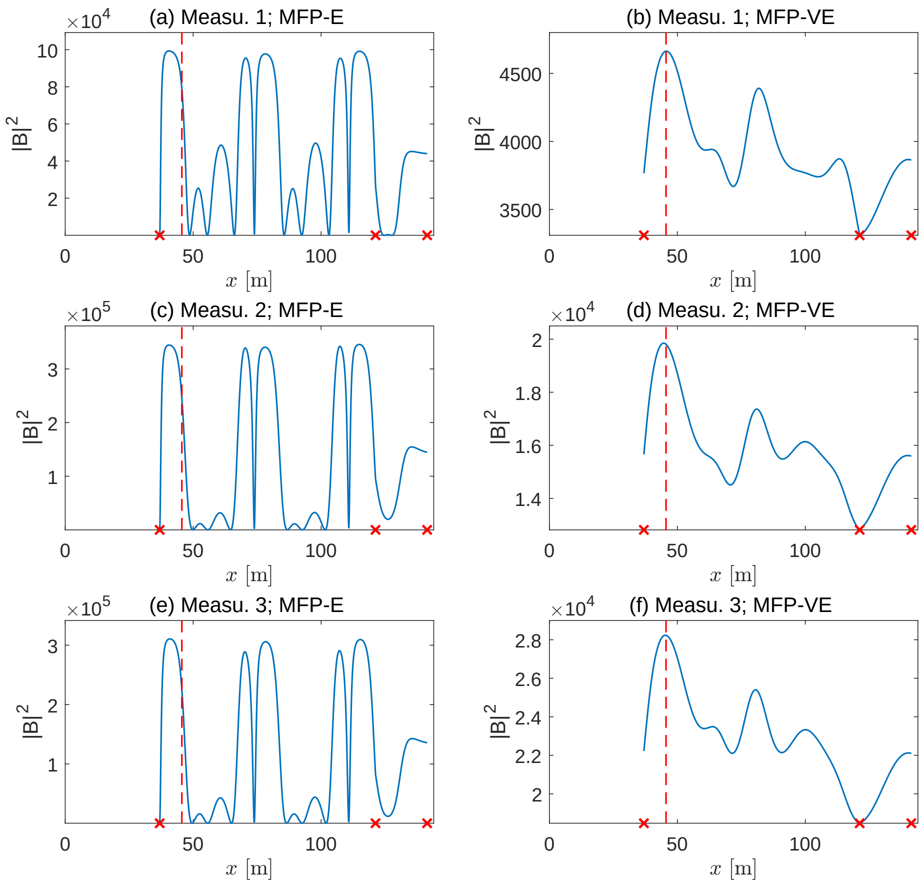

Figure 11: Leak localization using MFP-E (a,c,d) and MFP-VE (b,d,f). The three measurements shown in Figure 10 are respectively used.

- (a): MFP-VE (the method proposed in this paper) with all available frequencies $\omega \in [\omega_{th}, 17\omega_{th}]$.
- (b): MFP-VE (the method proposed in this paper) with only resonant frequencies, i.e., $\omega \in \{\omega_{th}, 3\omega_{th}, \cdots, 17\omega_{th}\}$.
- (c): MFP-E (the method in [21]) with all available frequencies $\omega \in [\omega_{th}, 17\omega_{th}]$.
- (d): MFP-E (the method in [21]) with only resonant frequencies, i.e., $\omega \in \{\omega_{th}, 3\omega_{th}, \cdots, 17\omega_{th}\}$.
- (e): The wavelet analysis method [5] (a representative of TRM) where the mother wavelet is the type Daubechies of order 1 (db1). It analyzes the drop due to leak in the first period of time signal from the hydrophone at x_1 and retains the largest drop as leak estimate.
- (f): The FRF peak pattern method [14, 16] (a representative of FRM; more specifically, a representative of resonant frequency based-method) which uses the peak frequencies $\omega \in \{\omega_{th}, 3\omega_{th}, \cdots, 17\omega_{th}\}$ of FRF of the hydrophone at x_1 as data for leak localization.
- (g): The inverse transient analysis (ITA) method [26] with consideration of viscoelastic effect [38]. Here, 51 potential leaks uniformally distributed in the pipe, i.e., $\{x : x = nl/50, n = 0, \cdots, 50\}$, and the sizes of the 51 potential leaks are estimated by solving a 51-parameter optimization problem. The one with highest leak size estimate is retained as leak location estimate. The measurements from all the three sensors are used. The information of actual leak location is used for the initialization of optimization (although it is not available in practice): for all the three cases of Q_0^L/Q_0, the initial leak size at the potential leak closest to the actual leak is 3.4×10^{-5} m^{-2}, while at the other potential leaks the initial sizes are all 0.

Figures 12, 13, and 14 show the box plots of absolute error of leak localization, denoted by $|e| = \left|\widehat{x^L} - x^L\right|$, in the cases of three leak sizes. Tables 4, 5, and 6 display the corresponding statistics $|e|$, including mean, standard deviation, maximum, minimum, and percentiles of $|e|$. The results illustrate that MFP-VE with all frequencies is very accurate in all the three cases of leak sizes. For example, for the smallest leak where $Q_0^L/Q_0 = 10\%$ the average error is only 0.56 m, the maximum error is 1.16 m, and in 49 over 50 tests the leak localization error is less than 1 m. The average error is lower for the larger leaks. Both considering viscoelasticity and using more frequencies are essential for accuracy of MFP leak localization: the methods (b), (c) and (d) all have much higher error than (a). The methods (e), (f) and (g) also have relatively large error of leak localization. It is remarkable that for the FRF peak pattern method (f), due to only nine FRF peaks are available, the resolution of leak localization is actually very low that leak location estimate can only be chosen from nine candidates along the pipe. Similarly, the resolution of ITA method (g) is decided by the distribution of potential leaks; here, the resolution of (g) is $l/100 = 1.44$ m because the leak is selected from $\{x : x = nl/50, n = 0, \cdots, 50\}$ (51 potential leaks are assumed in this case).

In practice, excavation cost is proportional to range of possible leak location, therefore leak localization with accuracy less than a threshold is of importance. Successful rate of leak localization in the sense of absolute error $|e|$ less than 1 m, 3 m, 5 m and 10 m, computed from the 50 water hammer experiments, is shown in Table 7. Again, MFP-VE with all frequencies (a) outperforms other methods. The wavelet method (e), which does not need many pipe parameters such as viscoelasticity coefficients, has error less than 5 m in most cases which is also acceptable in this sense.

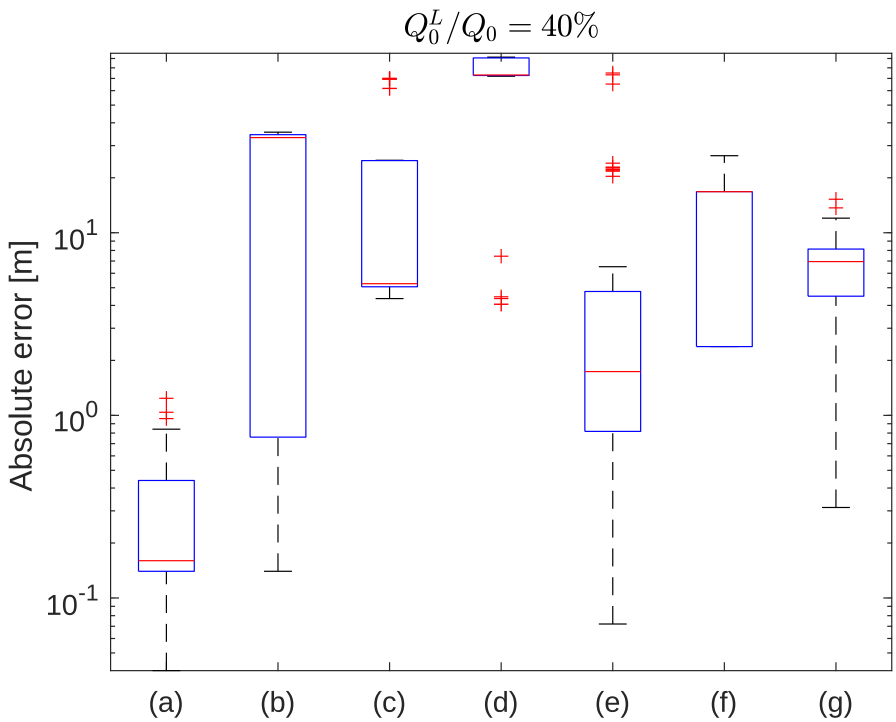

Figure 12: Box plot of absolute error of leak localization obtained from 50 water hammer experiments. The methods used for leak localization is (a) MFP-VE with all frequencies; (b) MFP-VE with only resonant frequencies; (c) MFP-E with all frequencies; (d) MFP-E with only resonant frequencies; (e) wavelet transform method; (f) FRF peak pattern method; (g) ITA method. The ratio Q_0^L/Q_0 of leak flow and main flow is 40%.

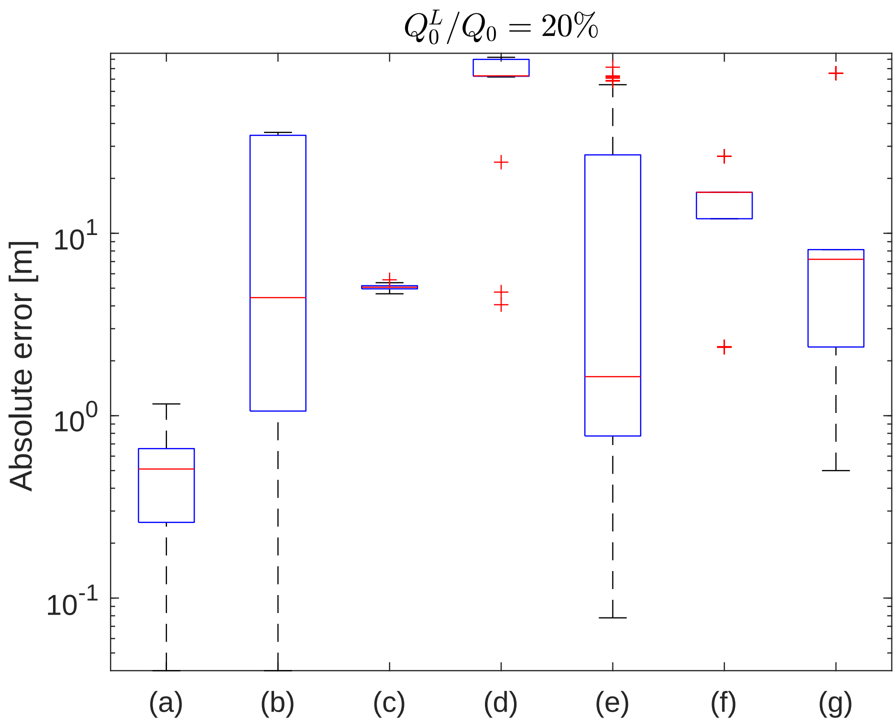

Figure 13: Box plot of absolute error of leak localization obtained from 50 water hammer experiments. The methods used for leak localization is (a) MFP-VE with all frequencies; (b) MFP-VE with only resonant frequencies; (c) MFP-E with all frequencies; (d) MFP-E with only resonant frequencies; (e) wavelet transform method; (f) FRF peak pattern method; (g) ITA method. The ratio Q_0^L/Q_0 of leak flow and main flow is 20%.

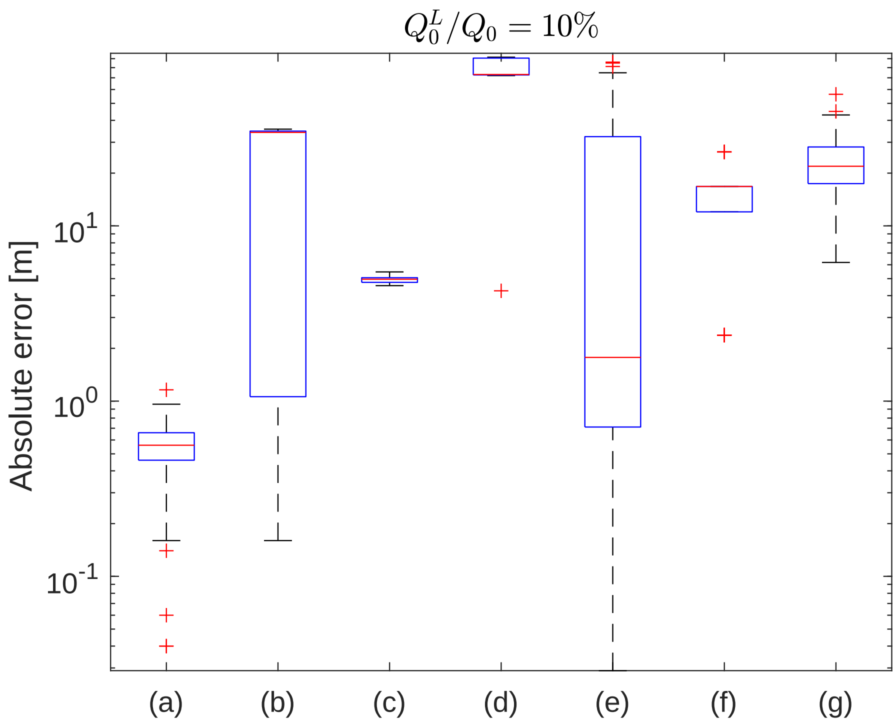

Figure 14: Box plot of absolute error of leak localization obtained from 50 water hammer experiments. The methods used for leak localization is (a) MFP-VE with all frequencies; (b) MFP-VE with only resonant frequencies; (c) MFP-E with all frequencies; (d) MFP-E with only resonant frequencies; (e) wavelet transform method; (f) FRF peak pattern method; (g) ITA method. The ratio Q_0^L/Q_0 of leak flow and main flow is 10%.

$\lvert e \rvert$	(a)	(b)	(c)	(d)	(e)	(f)	(g)
Mean [m]	0.29	19.49	20.17	73.16	8.89	13.43	6.47
Std. [m]	0.27	16.72	26.21	24.53	17.51	8.19	3.17
Max [m]	1.24	35.54	70.14	91.54	74.95	26.42	15.26
Min [m]	0.04	0.14	4.36	4.06	0.07	2.38	0.31
5% Percentile [m]	0.04	0.14	4.76	4.36	0.21	2.38	0.5
25% Percentile [m]	0.14	0.76	5.06	72.64	0.82	2.38	4.49
50% Percentile [m]	0.16	33.19	5.26	73.09	1.74	16.78	6.95
75% Percentile [m]	0.44	34.44	24.84 m	90.64	4.77	73.16	8.14
95% Percentile [m]	0.96	35.04	69.64 m	91.24	65.18	26.42	12.02

Table 4: Statistics of absolute error of leak localization obtained from 50 water hammer experiments. The methods used for leak localization is (a) MFP-VE with all frequencies; (b) MFP-VE with only resonant frequencies; (c) MFP-E with all frequencies; (d) MFP-E with only resonant frequencies; (e) wavelet transform method; (f) FRF peak pattern method; (f) FRF peak pattern method; (g) ITA method. The ratio Q_0^L/Q_0 of leak flow and main flow is 40%.

$\lvert e \rvert$	(a)	(b)	(c)	(d)	(e)	(f)	(g)
Mean [m]	0.52	17.15	5.05	74.16	17.60	14.10	12.15
Std. [m]	0.28	16.76	0.18	18.15	26.80	6.73	21.50
Max [m]	1.16	35.74	5.56	92.24	81.40	26.42	75.38
Min [m]	0.04	0.04	4.66	4.06	0.08	2.38	0.5
5% Percentile [m]	0.06	0.06	4.76	24.54	0.21	2.38	0.5
25% Percentile [m]	0.26	1.06	4.96	72.64	0.77	12.02	2.38
50% Percentile [m]	0.51	4.44	5.06	72.99	1.64	16.78	7.20
75% Percentile [m]	0.66	34.44	5.16	89.84	26.92	16.78	8.14
95% Percentile [m]	0.96	35.24	5.26	91.14	71.94	26.42	75.38

Table 5: Statistics of absolute error of leak localization obtained from 50 water hammer experiments. The methods used for leak localization is (a) MFP-VE with all frequencies; (b) MFP-VE with only resonant frequencies; (c) MFP-E with all frequencies; (d) MFP-E with only resonant frequencies; (e) wavelet transform method; (f) FRF peak pattern method; (g) ITA method. The ratio Q_0^L/Q_0 of leak flow and main flow is 20%.

$\|e\|$	(a)	(b)	(c)	(d)	(e)	(f)	(g)
Mean [m]	0.56	21.80	4.94	79.30	18.85	14.29	23.94
Std. [m]	0.24	16.51	0.21	14.08	29.14	6.74	10.61
Max [m]	1.16	35.64	5.46	91.74	85.98	26.42	56.34
Min [m]	0.04	0.16	4.56	4.26	0.03	2.38	6.18
5% Percentile [m]	0.06	0.16	4.66	72.24	0.03	2.38	9.47
25% Percentile [m]	0.46	1.06	4.76	72.64	0.71	12.02	17.43
50% Percentile [m]	0.56	34.14	4.96	73.09	1.78	16.78	21.89
75% Percentile [m]	0.56	34.74	5.06	90.64	32.31	16.78	28.20
95% Percentile [m]	0.96	35.54	5.26	91.44	81.20	26.42	42.94

Table 6: Statistics of absolute error of leak localization obtained from 50 water hammer experiments. The methods used for leak localization is (a) MFP-VE with all frequencies; (b) MFP-VE with only resonant frequencies; (c) MFP-E with all frequencies; (d) MFP-E with only resonant frequencies; (e) wavelet transform method; (f) FRF peak pattern method; (g) ITA method. The ratio Q_0^L/Q_0 of leak flow and main flow is 10%.

Q_0^L/Q_0	error	(a)	(b)	(c)	(d)	(e)	(f)	(g)
40%	≤ 1 m	96%	32%	0	0	32%	0	6%
	≤ 3 m	100%	44%	0	0	62%	28%	16%
	≤ 5 m	100%	44%	24%	8%	76%	28%	30%
	≤ 10 m	100%	44%	72%	10%	80%	28%	90%
20%	≤ 1 m	96%	24%	0	0	38%	0	20%
	≤ 3 m	100%	48%	0	0	60%	28%	28%
	≤ 5 m	100%	50%	38%	4%	64%	20%	38%
	≤ 10 m	100%	52%	100%	4%	66%	20%	90%
10%	≤ 1 m	98%	22%	0	0	34%	0	0
	≤ 3 m	100%	38%	0	0	58%	20%	0
	≤ 5 m	100%	38%	64%	2%	64%	20%	0
	≤ 10 m	100%	38%	100%	2%	68%	20%	16%

Table 7: Successful rate of leak localization computed from 50 water hammer experiments in the sense of absolute error less than 1 m, 3 m, 5 m and 10 m, respectively. The methods used for leak localization is (a) MFP-VE with all frequencies; (b) MFP-VE with only resonant frequencies; (c) MFP-E with all frequencies; (d) MFP-E with only resonant frequencies; (e) wavelet transaform method; (f) FRF peak pattern method; (g) ITA method.

5. Discussions

In this section, the experimental results and the leak localization methods are more profoundly discussed, in the following aspects.

- *Modeling physical complexity*: An advantage of the MFP approach proposed in this paper is that the algorithm includes the viscoelasticity effect of pipe wall, which largely modifies the behavior of transient wave in pipe and measured data. The physical model dependent methods like MFP can produce very accurate leak localization. However, its accuracy depends on the correctness of the physical model. When the elastic (wrong) model is used in the viscoelastic case, i.e., the methods (c) and (d), or the viscoelastic coefficients cannot be satisfactorily given, the localization is not accurate. In the case that accurate model is not available, methods less dependent on physical model, such as the wavelet method (e), is an option.

- *Sufficienct use of information from measurements*: It has been shown in the literature that many leak detection methods using partial information (reflection, resonant frequencies, etc.) work well in ideal environments. However, in real experiments which are usually very noisy and have many unknown uncertainties, the used partial information is very possibly contaminated such that these methods fail. A solution is to use as much information as possible. This paper experimentally justifies this issue: the method (a), which uses all available information, outperforms the method (b), which uses only resonant frequencies, and the method (e), which uses only the reflection due to leak in the first period. This issue has also been justified numerically in [21] and theoretically via the theory of Fisher information and Cramér-Rao lower bound (CRLB) [22, 51]: each time step of the time signal or each frequency in the FRF are useful information for leak detection and decreases the expected estimation error.

- *Multi-sensor fusion*: Again, due to the presence of noise and uncertainty, it is preferable to use as much information as possible. Except using more frequencies and time signals, another approach is to set more sensors in the pipe. MFP (as well as ITA) is able to fuse information from different sensors, without changing the algorithm but only increases the length of the vectors $\Delta\mathbf{h}$ and $\mathbf{G}$ in Eq. (36). On the other hand, MFP needs at least three sensors, while the other three methods (e), (f) and (g) can be used if only one sensor is available, which provides more flexibility.

- *Computation complexity*: MFP and ITA has the similarity that both methods decide the leak by matching the measured data with the physical model. However, ITA needs to solve a multiple-parameter optimization problem; its dimension equals to the number of potential leaks assumed in the pipe. Therefore, a high localization resolution or precision of ITA implies an extremely slow computation and vice versa. Also, the result of ITA strongly depends on the initial value and it is very possible that the algorithm stops at local maximum which corresponds to a bad result. By contrast, the matching of MFP only needs to solve a 1D optimization, therefore a 1D search/plot of MFP objective function versus leak location along the pipe is sufficient. This implies that MFP has a fast computation, does not need initial guess of leak, and avoids local maximum traps.

The above discussion regarding the properties of the leak localization methods is briefly summarized in Table 8.

	MFP	Wavelet	Peak pattern	ITA
Modeling viscoelasiticy	Yes	No	No	Yes
Sufficient use of signal	Yes	No	No	Yes
Initial parameter	No	No	No	Yes
Computation speed	Fast	Fast	Fast	Slow
Using multiple sensors	Yes	No	No	Yes
Minimum sensor number	3	1	1	1

Table 8: Summary of the properties of the leak localization methods.

6. Conclusion

This paper addresses the problem of leakage detection in a viscoelastic pipe. The viscoelasticity of pipe wall is modeled in the governing equations of transient wave and, in the frequency domain, the viscoelastic effect is equivalent to modifying the transfer matrix with a frequency-dependent wave speed. Then, Matched-field processing (MFP), which has been proposed for leakage detection in elastic pipes, is generalized for the viscoelastic case.

Transient experiment results with viscoelastic pipe in the Water Engineering Laboratory at University of Perugia and in the Water Resources Research Laboratory at Hong Kong University of Science and Technology are both studied to justify the proposed method. It is shown that both considering pipe wall viscoelasticity and using more frequencies (instead of using only the resonant frequencies) in the leakage localization scheme are essential for leak localization accuracy. The proposed MFP method outperforms classical leakage detection methods in the literature in the sense of smaller leak localization error. For a small leak where the flow ratio of leak and main pipe is 10%, MFP is very accurate that, in 49 of 50 experiments, the leak localization error is lower than 1 m (the error of the rest one is 1.14 m), although some of these signals are seriously contaminated by noise and uncertainties.

Further work may be conducted in several directions. First, the generalization of the results to more complicated cases, for example localization of multiple leaks and application to more complex piping systems, would be important. Besides, this paper uses the pipe wall viscoelastic coefficients obtained from a no-leak test, which may not be available in some practical cases. Therefore, a more advanced method that can jointly estimate leaks and the viscoelastic coefficients would be interesting.

Acknowledgements

This work has been supported by research grants from the Research Grant Council of the Hong Kong SAR, China (Project No. T21-602/15R). The authors would like to thank Duncan A. McInnis, Asgar Ahadpour Dodaran, Man Yue Lam, Moez Louati, Muhammad Waqar, and Kamrun Nahar Keya for their helps on the experiments at HKUST.

References

[1] A. F. Colombo, P. Lee, and B. W. Karney. A selective literature review of transient-based leak detection methods. *Journal of Hydro-Environment Research*, 2(4):212–227, 2009.

[2] B. Brunone. Transient test-based technique for leak detection in outfall pipes. *Journal of Water Resources Planning and Management*, 125(5):302–306, 1999.

[3] B. Brunone and M. Ferrante. Detecting leaks in pressurised pipes by means of transients. *Journal of Hydraulic Research*, 39(5):539–547, 2001.

[4] D. Covas, H. Ramos, N. Graham, and C. Maksimovic. Application of hydraulic transients for leak detection in water supply systems. *Water Science and Technology: Water Supply*, 4(5-6):365–374, 2005.

[5] M. Ferrante, B. Brunone, and S. Meniconi. Wavelets for the analysis of transient pressure signals for leak detection. *Journal of Hydraulic Engineering*, 133(11):1274–1282, 2007.

[6] S. Meniconi, B. Brunone, M. Ferrante, C. Capponi, C. A. Carrettini, C. Chiesa, D. Segalini, and E. A. Lanfranchi. Anomaly pre-localization in distribution–transmission mains by pump trip: preliminary field tests in the milan pipe system. *Journal of Hydroinformatics*, 17(3):377–389, 2015.

[7] S. T. N. Nguyen, J. Gong, M. F. Lambert, A. C Zecchin, and A. R. Simpson. Least squares deconvolution for leak detection with a pseudo random binary sequence excitation. *Mechanical Systems and Signal Processing*, 99:846–858, 2018.

[8] X.-J. Wang, M. F. Lambert, A. R. Simpson, J. A. Liggett, and J. P. Vítkovskỳ. Leak detection in pipelines using the damping of fluid transients. *Journal of Hydraulic Engineering*, 128(7):697–711, 2002.

[9] J. C. P. Liou. Pipeline leak detection by impulse response extraction. *Journal of Fluids Engineering*, 120(4):833–838, 1998.

[10] W. Mpesha, S. L. Gassman, and M. H. Chaudhry. Leak detection in pipes by frequency response method. *Journal of Hydraulic Engineering*, 127(2):134–147, 2001.

[11] M. Ferrante and B. Brunone. Pipe system diagnosis and leak detection by unsteady-state tests. 1. harmonic analysis. *Advances in Water Resources*, 26(1):95–105, 2003.

[12] D. Covas, H. Ramos, and A. B. De Almeida. Standing wave difference method for leak detection in pipeline systems. *Journal of Hydraulic Engineering*, 131(12):1106–1116, 2005.

[13] P. J. Lee, J. P. Vitkovsky, M. F. Lambert, A. R. Simpson, and J. A. Liggett. Frequency response coding for the location of leaks in single pipeline systems. *The Int. Conference on Pumps, Electromechanical Devices and Systems Applied to Urban Water Management, IAHR and IHRA, Valencia, Spain, April 22-25*, 2003.

[14] P. J. Lee, J. P. Vítkovskỳ, M. F. Lambert, A. R. Simpson, and J. A. Liggett. Leak location using the pattern of the frequency response diagram in pipelines: a numerical study. *Journal of Sound and Vibration*, 284(3):1051–1073, 2005.

[15] P. J. Lee, J. P. Vítkovskỳ, M. F. Lambert, A. R. Simpson, and J. A. Liggett. Frequency domain analysis for detecting pipeline leaks. *Journal of Hydraulic Engineering*, 131(7):596–604, 2005.

[16] P. J. Lee, M. F. Lambert, A. R. Simpson, J. P. Vítkovskỳ, and J. Liggett. Experimental verification of the frequency response method for pipeline leak detection. *Journal of Hydraulic Research*, 44(5):693–707, 2006.

[17] A. M. Sattar and M. H. Chaudhry. Leak detection in pipelines by frequency response method. *Journal of Hydraulic Research*, 46(EI1):138–151, 2008.

[18] M. Taghvaei, S. B. M. Beck, and J. B. Boxall. Leak detection in pipes using induced water hammer pulses and cepstrum analysis. *International Journal of COMADEM*, 13(1):19, 2010.

[19] H.-F. Duan, P. J. Lee, M. S. Ghidaoui, and Y.-K. Tung. Leak detection in complex series pipelines by using the system frequency response method. *Journal of Hydraulic Research*, 49(2):213–221, 2011.

[20] I. Rubio Scola, G. Besançon, and D. Georges. Blockage and leak detection and location in pipelines using frequency response optimization. *Journal of Hydraulic Engineering*, 143(1):04016074, 2016.

[21] X. Wang and M. S. Ghidaoui. Pipeline leak detection using the matched-field processing method. *Journal of Hydraulic Engineering*, 144 (6):04018030, 2018.

[22] X. Wang and M. S. Ghidaoui. Identification of multiple leaks in pipeline: Linearized model, maximum likelihood, and super-resolution localization. *Mechanical Systems and Signal Processing*, 107:529–548, 2018.

[23] X. Wang, D. P. Palomar, L. Zhao, M. S. Ghidaoui, and R. D. Murch. Spectral-based methods for pipeline leakage detection. *Journal of Hydraulic Engineering*, In press, DOI: 10.1061/(ASCE)HY.1943-7900.0001572, 2019.

[24] X. Wang and M. S. Ghidaoui. Identification of multiple leaks in pipeline II: Iterative beamforming and leak number estimation. *Mechanical Systems and Signal Processing*, 119:346–362, 2019.

[25] B. Zhou, A. Liu, X. Wang, Y. She, and V. Lau. Compressive sensing-based multiple-leak identification for smart water supply systems. *IEEE Internet of Things Journal*, 5 (2):1228–1241, 2018.

[26] J. A. Liggett and L.-C. Chen. Inverse transient analysis in pipe networks. *Journal of Hydraulic Engineering*, 120(8):934–955, 1994.

[27] J. P. Vítkovskỳ, A. R. Simpson, and M. F. Lambert. Leak detection and calibration using transients and genetic algorithms. *Journal of Water Resources Planning and Management*, 126(4):262–265, 2000.

[28] M. L. Stephens. *Transient response analysis for fault detection and pipeline wall condition assessment in field water transmission and distribution pipelines and networks.* PhD Thesis, University of Adelaide, 2008.

[29] D. Covas and H. Ramos. Case studies of leak detection and location in water pipe systems by inverse transient analysis. *Journal of Water Resources Planning and Management*, 136(2):248–257, 2010.

[30] P. G. Franke. Computation of unsteady pipe flow with respect to visco-elastic material properties. *Journal of Hydraulic Research*, 21(5):345–353, 1983.

[31] G. Pezzinga and P. Scandura. Unsteady flow in installations with polymeric additional pipe. *Journal of Hydraulic Engineering*, 121(11):802–811, 1995.

[32] D. Covas, I. Stoianov, H. Ramos, N. Graham, and C. Maksimovic. The dynamic effect of pipe-wall viscoelasticity in hydraulic transients. part iexperimental analysis and creep characterization. *Journal of Hydraulic Research*, 42(5):517–532, 2004.

[33] D. Covas, I. Stoianov, J. F. Mano, H. Ramos, N. Graham, and C. Maksimovic. The dynamic effect of pipe-wall viscoelasticity in hydraulic transients. part iimodel development, calibration and verification. *Journal of Hydraulic Research*, 43(1):56–70, 2005.

[34] A. Keramat, A. S. Tijsseling, Q. Hou, and A. Ahmadi. Fluid-structure interaction with pipe-wall viscoelasticity during water hammer. *Journal of Fluids and Structures*, 28:434–455, 2012.

[35] H.-F. Duan, M. Ghidaoui, P. J. Lee, and Y.-K. Tung. Unsteady friction and visco-elasticity in pipe fluid transients. *Journal of Hydraulic Research*, 48(3):354–362, 2010.

[36] H.-F. Duan, P. J. Lee, M. S. Ghidaoui, and Y.-K. Tung. System response function–based leak detection in viscoelastic pipelines. *Journal of Hydraulic Engineering*, 138(2):143–153, 2011.

[37] S. Meniconi, B. Brunone, M. Ferrante, and C. Massari. Numerical and experimental investigation of leaks in viscoelastic pressurized pipe flow. *Drinking Water Engineering and Science*, 6(1):11, 2013.

[38] A. K. Soares, D. I. C. Covas, and Luisa Fernanda R. R. Leak detection by inverse transient analysis in an experimental pvc pipe system. *Journal of Hydroinformatics*, 13(2):153–166, 2011.

[39] M. T. Shaw and W. J. MacKnight. *Introduction to Polymer Viscoelasticity*. John Wiley & Sons, 2005.

[40] P. J. Lee and J. P. Vítkovskỳ. Quantifying linearization error when modeling fluid pipeline transients using the frequency response method. *Journal of Hydraulic Engineering*, 136(10):831–836, 2010.

[41] M. H. Chaudhry. *Applied Hydraulic Transients, Third Edition*. Springer, 2014.

[42] E. B. Wylie, V. L. Streeter, and L. Suo. *Fluid transients in systems*, volume 1. Prentice Hall Englewood Cliffs, NJ, 1993.

[43] A. Kashima, P. J Lee, and R. Nokes. Numerical errors in discharge measurements using the KDP method. *Journal of Hydraulic Research*, 50(1):98–104, 2012.

[44] A. Kashima, P. J. Lee, M. S. Ghidaoui, and M. Davidson. Experimental verification of the kinetic differential pressure method for flow measurements. *Journal of Hydraulic Research*, 51(6):634–644, 2013.

[45] A. Dubey, Z. Li, P. J. Lee, and R. Murch. Observations of acoustic noise in water supply pipeline systems. *Journal of the Acoustical Society of America*, Under Review, 2019.

[46] J. Lin, X. Wang, and M. S. Ghidaoui. Theoretical investigation of leak's impact on normal modes of a water-filled pipe: from small to large leak impedance. *Journal of Hydraulic Engineering*, In press, DOI: 10.1061/(ASCE)HY.1943-7900.0001606, 2019.

[47] P. J. Lee. *Using system response functions of liquid pipelines for leak and blockage detection*. PhD Thesis. The University of Adelaide, Adelaide AU, 2005.

[48] P. A. Lynn. *An introduction to the analysis and processing of signals*. McMillan, 1973.

[49] G. Pezzinga, B. Brunone, and S. Meniconi. Relevance of pipe period on Kelvin-Voigt viscoelastic parameters: 1D and 2D inverse transient analysis. *Journal of Hydraulic Engineering*, 142(12):04016063, 2016.

[50] M. Ferrante, B. Brunone, S. Meniconi, B. W. Karney, and C. Massari. Leak size, detectability and test conditions in pressurized pipe systems. *Water resources management*, 28(13):4583–4598, 2014.

[51] A. Keramat, M. S. Ghidaoui, X. Wang, and M. Louati. Cramer-Rao lower bound for performance analysis of leak detection. *Journal of Hydraulic Engineering, under review*, In press, DOI: 10.1061/(ASCE)HY.1943-7900.0001603, 2019.